

Subwavelength binary plasmonic solitons

Yao Kou* and Jens Förstner

Department of Electrical Engineering, University of Paderborn, Warburger Str. 100, 33098 Paderborn, Germany

*Corresponding author: yao.kou@uni-paderborn.de

Received December 11, 2014; revised January 30, 2015; accepted January 31, 2015;
posted February 2, 2015 (Doc. ID 230587); published March 2, 2015

We study the formation of subwavelength solitons in binary metal-dielectric lattices. We show that the transverse modulation of the lattice constant breaks the fundamental plasmonic band and suppresses the discrete diffraction of surface plasmon waves. New types of plasmonic solitons are found, and their characteristics are analyzed. We also demonstrate the existence of photonic-plasmonic vector solitons and elucidate their propagation properties. © 2015 Optical Society of America

OCIS codes: (190.4390) Nonlinear optics, integrated optics; (250.5403) Plasmonics; (190.6135) Spatial solitons.

<http://dx.doi.org/10.1364/OL.40.000851>

Periodic photonic structures, e.g., photonic crystals and optical waveguide arrays (lattices), have been considered as an excellent platform to achieve efficient control on the light flow. These discontinuous environments give rise to abundant optical dynamics that only exist in the discrete systems. Typical discrete optical effects, such as diffraction management [1], Bloch oscillations [2], and dynamical localization [3], have been theoretically and experimentally demonstrated. In nonlinear lattices, types of discrete optical solitons have also been revealed [4,5], including surface solitons [6,7], gap solitons [8–10], and vector solitons [11–13].

Although discrete optics has been under investigation for many years, only recently the advance of nanofabrication techniques pushed the study toward subwavelength scale systems. A particularly appealing example are plasmonic lattices, in which new phenomena, including negative coupling [14–18], reversed diffraction relation [15–18], and subwavelength light dynamical localization [19], have been discovered. More importantly, the use of plasmonic structures makes it possible to overcome the optical diffraction limit. It was thus suggested that lattice solitons can be supported with a characteristic dimension well below the light wavelength, providing important opportunities for the nanoscale all-optical manipulations [15–18,20–22]. However, due to the strong tunneling of plasmonic waves across the lattices, a giant nonlinear refractive index is usually required by a deeply localized wave packet to counteract the transverse diffraction, which might hinder the experimental realization of such subwavelength entities.

In this Letter, we report the effect of diffraction suppression given rise by a transverse binary modulation on plasmonic lattices and study its influence on the properties of plasmonic solitons. Light dynamics in binary photonic structures has received much attention during the past years due to its fundamental interest in different branches of optics [23–25], among which of particular interest is the generation of binary solitons, which exhibit unique properties in comparison with conventional discrete solitons [26–31]. Up to now, binary solitons have only been considered in diffraction-limited dielectric systems, in which light propagation can be properly described by scalar equations under the paraxial approximation. The approximation, however, is no longer valid for subwavelength beams since their vectorial field nature must be taken into

account [5]. From this point, we extend the study into nanoscale systems by solving the full Maxwell equations (MEs) in a dissipative nonlinear plasmonic lattice. We demonstrate how the binarization influences the plasmonic band-gap spectrum and the associated nonlinear modes. As a result of diffraction suppression, the modes exhibit compact confinement under a significantly reduced nonlinearity level. We find that the proposed setting supports two types of photonic-plasmonic vector solitons, in which the strength of mutual trapping is decided by the originating band of the plasmonic mode.

We consider light propagating in an array of metal-dielectric slits, as depicted in Fig. 1(a), where nanoscale dielectric layers with alternative widths of d_1 and d_2 are separated by metallic layers with a fixed width of $d_m = 50$ nm. The period of the lattice, along x axis, is hence $p = d_1 + d_2 + 2d_m$, while light travels along z axis. We assume a Kerr-type nonlinearity for the dielectric refractive index as $n_d = n_0 + \delta n = n_0 + n_2|E|^2$, where n_0 is the linear refractive index and n_2 the self-focusing ($n_2 > 0$) or self-defocusing ($n_2 < 0$) nonlinearity coefficient. The permittivity of metal (silver) is $\epsilon_m = -129 + 3.28i$ at the operation wavelength of $\lambda = 1550$ nm [32].

To analyze the diffraction property of the present lattice, we start by solving MEs in the linear case ($n_2 = 0$), where the propagation equations for TM-polarized waves ($E_y = H_x = H_z = 0$) can be readily described by [15]:

$$\frac{\partial E_x}{\partial z} = \frac{i}{\omega \epsilon_0} \frac{\partial}{\partial x} \left(\frac{1}{\epsilon_r} \frac{\partial H_y}{\partial x} \right) + i\omega \mu_0 H_y \quad (1)$$

$$\frac{\partial H_y}{\partial z} = i\omega \epsilon_0 \epsilon_r E_x, \quad \frac{\partial H_y}{\partial x} = -i\omega \epsilon_0 \epsilon_r E_z. \quad (2)$$

Here $\omega = 2\pi c/\lambda$ is the light angular frequency; $\epsilon_r(x)$ is the spatial modulation on the relative permittivity, with $\epsilon_r = \epsilon_m$ in metal and $\epsilon_r = \epsilon_d = n_d^2$ in dielectric media. Assuming Bloch modes in the form $[E_x, H_y] = [A(x), B(x)]e^{i(\beta z - \omega t)}$, with β being the Bloch wave vector and $[A(x+p), B(x+p)] = [A(x), B(x)]e^{ik_x p}$, from Eqs. (1) and (2), we can calculate the transmission spectrum for linear TM modes. The transmission spectrum for TE modes ($E_x = E_z = H_y = 0$) can be analogously obtained using the TE-based propagation equations, despite the fact that only the bands associated with fundamental

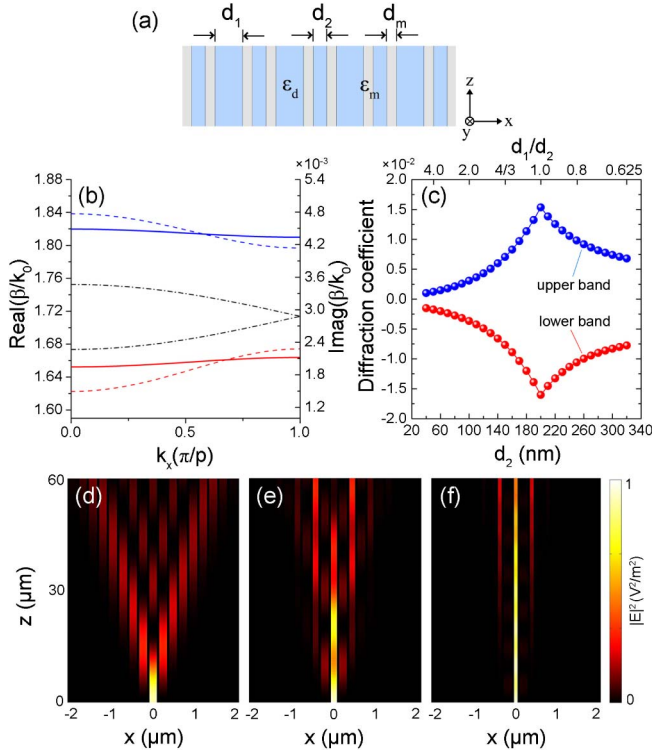


Fig. 1. (a) Sketch of the present binary plasmonic lattice. (b) Real (solid curves) and imaginary (dashed curves) parts of the propagation constant β vs. k_x , for $n_0 = 1.5$, $d_1 = 200$ nm, $d_2 = 100$ nm. Blue curves: upper band, red curves: lower band, dashed-dotted curves: real part of fundamental band for a uniform lattice with $d_1 = d_2 = 150$ nm. (c) Diffraction coefficient vs. d_2 , for $d_1 = 200$ nm. (d)-(f) Linear propagation in plasmonic lattice with central-waveguide excitation, where $d_1 = 200$ nm and (d) $d_2 = 200$ nm, (e) $d_2 = 150$ nm, (f) $d_2 = 100$ nm.

symmetric TM mode (referring to E_x) can survive in the deep-subwavelength scale.

Figure 1(b) shows the band-gap structure for TM modes with $d_1 = 200$ nm and $d_2 = 100$ nm. For comparison, the fundamental band for a uniform lattice with the same period is also illustrated (dashed-dotted curves). One can see that, as a direct consequence of the transverse modulation, a transmission gap emerges and separates the fundamental band into two sub-bands (here denoted as “upper” and “lower” band, respectively). Note that for the given parameters, bands associated with higher-order modes have been well cut-off. A similar scenario of band splitting was also encountered in Ref. [33] through tuning the coupling strength across metal slits and was qualitatively described under the paraxial-model. As an important feature in our scheme, guided modes are trapped by a binary-type potential provided by the alternate dielectric width, which leads to a selective concentration of the field amplitude in either wide or narrow waveguides, characterized by its originating band. One can see that as the ratio of d_1 to d_2 increases, both the sub-bands become less steep, and the width of the gap grows, indicating a decrease of the diffraction coefficient $-\partial^2\beta/\partial k_x^2$. In Fig. 1(c), we plot the variation of diffraction coefficients (at $k_x = 0$) with d_2 , where d_1 is fixed as 200 nm. Over five times diffraction suppression

is observed for both the sub-bands as d_2 changes from 200 nm (uniform lattice) to 20 nm. This result is further proven by direct propagation simulations in linear lattices with a single-site excitation, as illustrated in Figs. 1(d)–1(f), where the lattice ratio is chosen as $d_1/d_2 = 1, 4/3$ and 2, respectively, and light is input from the central narrow waveguide. The diffraction length clearly increases in the deep-modulated lattices, showing that the energy exchange across the lattice period has been significantly weakened in this case.

We now analyze the nonlinear version of the binary lattice with $|n_2| = 3.6 \times 10^{-21}$ m²/V² and seek for spatially localized solutions of Eqs. (1) and (2) in the form

$$E_x(x, z, t) = u(x)e^{i(\beta z - \omega t)} \quad (3)$$

$$H_y(x, z, t) = v(x)e^{i(\beta z - \omega t)}. \quad (4)$$

Substitution of Eqs. (3) and (4) into the MEs leads to a set of linear equations for the field distribution $u(x)$ and $v(x)$, which can be solved with a self-consistent method [11,15]. We find that, for each sign of n_2 , two categories of solitons are supported: the first category [Type-i and -iv, see Fig. 2(a)] resides in the semi-infinite gaps and is analogous to the fundamental modes in uniform lattices, whereas the second category (Type-ii and -iii), generating inside the gap, can only be found under the binary configuration. The existence of these solitons in band-gap spectrum can be characterized by their power, $P = (1/2) \int \text{Re}(E_x H_y^*) dx$, versus soliton propagation constant β . Figure 2(a) shows that the newly generated gap modes directly bifurcate from the linear propagation bands and penetrate into the deep gap region as the nonlinearity (soliton power) increases. However, in a reality consideration, their existence domain will actually be restricted by the experimentally achievable level of δn . For the case of a moderate nonlinear index of $|\delta n| = 0.005$, the gap soliton carries power of 329 W/ μm for the self-defocusing nonlinearity (Type-ii), and a higher value of 858 W/ μm for the self-focusing nonlinearity (Type-iii).

One typical property of the binary plasmonic solitons is that for the solitons bifurcating from the upper band, energy concentrates mainly in the narrow waveguides, while for those bifurcating from lower band, most energy localizes in the wide waveguides. As expected, solitons at $k_x = 0$ and $k_x = \pi/p$ exhibit in-phase and out-of-phase patterns, respectively, along the neighboring periods [see Figs. 2(b)–2(e)]. On the other hand, at the interface of each neighboring wide-narrow waveguides, a π (0) phase shift can be found for the Type-i (iv) plasmonic solitons, which is in contrast to the dielectric case and can be attributed to the negative coupling in plasmonic lattices. Numerical calculations also verify that soliton profiles are not obviously influenced by the imaginary part of metal permittivity if it is much smaller than the real part, which holds in our case.

To characterize the localization degree of the above nonlinear modes, the *effective soliton diameter* is introduced by $D = \sqrt{\int x^2 (|E_x|^2 + |E_z|^2) dx / \int (|E_x|^2 + |E_z|^2) dx}$. As an example, Fig. 2(d) compares the dependence of D on δn for the Type-i binary solitons and the

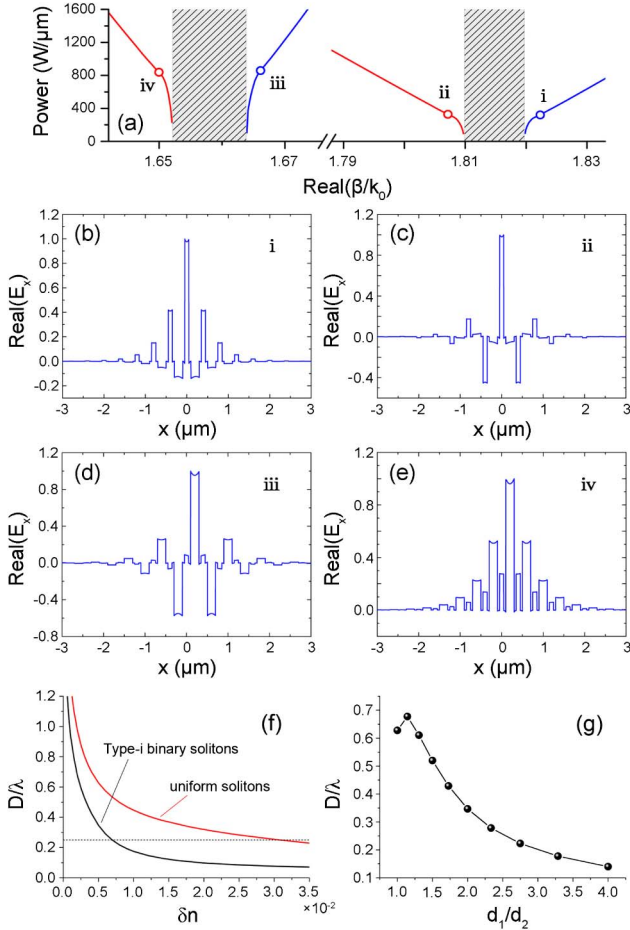


Fig. 2. (a) Soliton power vs. propagation constant. The blue (red) curves correspond to the self-focusing (self-defocusing) nonlinearity. The circles represent solitons for $|\delta n| = 0.005$. (b), (c) Normalized electric field profiles of the (b) Type-i, (c) Type-ii, (d) Type-iii, and (e) Type-iv solitons, $|\delta n| = 0.005$. (f) Soliton effective diameter vs. δn for Type-i binary solitons and uniform solitons. In (a)–(f): $d_1 = 200$ nm, $d_2 = 100$ nm. (g) Soliton effective diameter vs. d_1/d_2 for Type-i solitons, $d_1 + d_2 = 300$ nm, $\delta n = 0.005$.

corresponding uniform solitons ($d_1 = d_2 = 150$ nm). We find that the requirement on nonlinearity to form a sub-wavelength soliton is considerably reduced under the binary geometry, due to the diminished discrete diffraction. For instance, to realize a deep-localization of $D = 0.25\lambda$, δn drops from 0.032 to 0.007, while the corresponding power decreases tenfold from 3.75×10^3 W/ μm to 383 W/ μm . This expands the opportunity for practical use of such subwavelength solitons as only few nonlinear materials allow δn on the order of 10^{-2} [34]. To gain a clearer insight into how the modulation depth influences the soliton size, we further examine the D dependence of Type-i solitons on the ratio of d_1/d_2 , with $d_1 + d_2$ being fixed to be 300 nm [Fig. 2(e)]. One sees that, for $d_1/d_2 \geq 8/7$, the soliton size shrinks rapidly as the ratio grows, with most energy being compressed into the central (narrow) waveguide. The slight increase of D at small ratio can be understood by the energy transportation from wide waveguides to the next-to-center narrow waveguides under the shallow modulation. Note that although using dielectric material

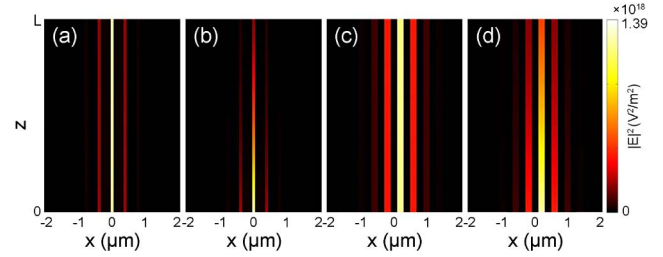


Fig. 3. (a), (b) Propagation of Type-i soliton in (a) lossless or (b) lossy plasmonic lattices. (c), (d) Propagation of Type-iii soliton in (c) lossless or (d) lossy plasmonic lattices. The propagation length is (a), (c) $L = 100$ μm , (b), (d) $L = 50$ μm .

with higher linear refractive-index can serve as an alternative way to compress soliton size to some extent, the accompanied drawback of doing that is a significant enhancement of the absorption loss, due to the increased imaginary part of soliton propagation constant. In our present case, the Type-i and Type-iv solitons feature the shortest (26 μm) and the longest (79 μm) propagation length, respectively, evaluated by $PL = 1/[2\text{Im}(\beta)]$. The loss can be entirely compensated by applying optical gain in the dielectric layers. For example, lossless propagation of the Type-i soliton requires a gain of 308 cm^{-1} , which can be easily achieved with dye molecules or quantum dots.

We now examine the soliton evolution by injecting the calculated mode profiles into the corresponding nonlinear lattices. The simulations are performed using a FEM software package COMSOL Multiphysics. Representative examples are given in Fig. 3, showing the propagation of Type-i and Type-iii (gap) solitons. One can observe the good maintenance of their profiles over tens of micrometers, even if the realistic metallic loss is present.

Finally, let us consider the formation of vector solitons in such binary lattices. Specifically, the vector states are searched as the combination of a TM plasmonic mode interacting with a TE photonic mode, i.e., $n_d = n_0 + \delta n = n_0 + n_2(|E_{\text{TM}}|^2 + |E_{\text{TE}}|^2)$. The TM component originates from either the upper or lower band and accordingly locates in the narrow or wide waveguides, whereas the TE component, which has a cut-off frequency, can only be supported by the wide waveguides. Therefore, the fundamental TE mode does not experience band splitting, but its diffraction coefficient is dramatically reduced due to the binarization. Figure 4(a) shows the

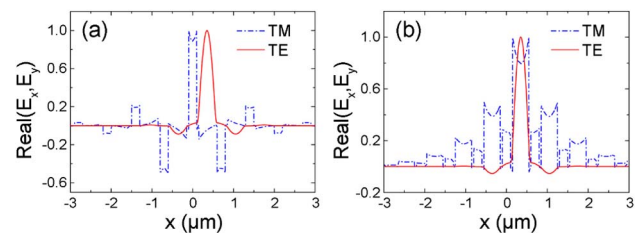


Fig. 4. Normalized electric field profiles of vector solitons for $\delta n_{\text{TM}} = \delta n_{\text{TE}} = -0.005$. The TM mode bifurcates from (a) upper and (b) lower band. $n_0 = 2.5$, $d_1 = 400$ nm, $d_2 = 200$ nm.

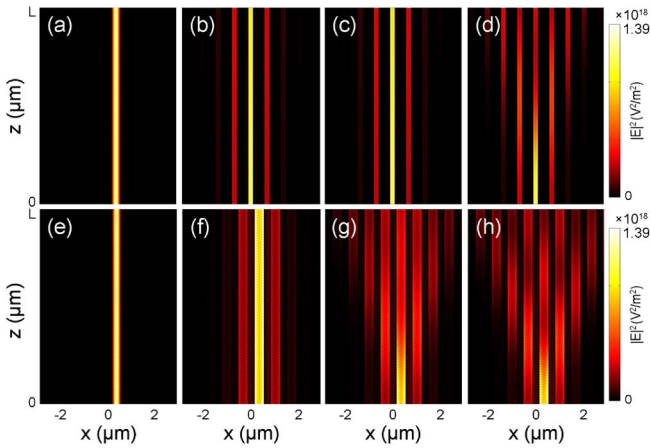


Fig. 5. Propagation of vector solitons. (a), (b) Stationary propagation of (a) TE mode and (b) TM mode of the soliton shown in Fig. 4(a). (c) Evolution of TM mode when TE mode are switched off. (d) The discrete diffraction of TM mode in linear lattice. (e)–(h) The same as (a)–(d) but for the vector soliton shown in Fig. 4(b). The propagation length in all the panels is $L = 200 \mu\text{m}$. The loss has been eliminated to clearly show the evolution properties.

typical profile of vector solitons where the Type-ii TM mode centering in the narrow waveguide possesses equal intensity to the TE mode as $\delta n_{\text{TM}} = \delta n_{\text{TE}} = -0.005$. The corresponding propagation dynamics is illustrated in Figs. 5(a)–5(d). Interestingly, since the two components occupy different channels of the same period and have only small overlapping, switching off one of the component (e.g., TE wave) does not noticeably impact the solitary propagation of the other [see Fig. 5(c)]. This indicates that nonlinear control of bi-polarized beams can be simultaneously realized in the same spot of a nanoscale lattice excluding remarkable cross-phase modulation, which could find interesting applications in photonic integrations.

On the other hand, conventional vector solitons can also form between the fundamental TE mode and the TM modes bifurcating from lower band, as depicted in Fig. 4(b). In this case, both components have their maximum amplitude in the wide waveguide and thus create a strong mutual trapping potential similar to the case in uniform waveguide arrays. This is verified by the observation of their dynamic evolution [Figs. 5(e)–5(h)], which shows that solitary propagation occurs only if both the components exist. On the contrary, switching off the TE component will totally destroy the stability of the TM part, where significant diffraction comparable to linear wave can be found [Fig. 5(g)].

In conclusion, we demonstrate significant diffraction suppression and band splitting in modulated plasmonic lattices. Compact solitons are found under a relatively small nonlinearity level. We also reveal the existence of photonic-plasmonic vector solitons in the present lattices.

This work has been supported by the Deutsche Forschungsgemeinschaft (DFG) via TRR142.

References

- H. Eisenberg, Y. Silberberg, R. Morandotti, and J. Aitchison, *Phys. Rev. Lett.* **85**, 1863 (2000).
- R. Morandotti, U. Peschel, J. Aitchison, H. Eisenberg, and Y. Silberberg, *Phys. Rev. Lett.* **83**, 4756 (1999).
- S. Longhi, M. Marangoni, M. Lobino, R. Ramponi, P. Laporta, E. Cianci, and V. Foglietti, *Phys. Rev. Lett.* **96**, 243901 (2006).
- F. Lederer, G. I. Stegeman, D. N. Christodoulides, G. Assanto, M. Segev, and Y. Silberberg, *Phys. Rep.* **463**, 1 (2008).
- Y. V. Kartashov, B. A. Malomed, and L. Torner, *Rev. Mod. Phys.* **83**, 247 (2011).
- K. G. Makris, S. Suntsov, D. N. Christodoulides, G. I. Stegeman, and A. Hache, *Opt. Lett.* **30**, 2466 (2005).
- S. Suntsov, K. G. Makris, D. N. Christodoulides, G. I. Stegeman, A. Hache, R. Morandotti, H. Yang, G. Salamo, and M. Sorel, *Phys. Rev. Lett.* **96**, 063901 (2006).
- Y. S. Kivshar, *Phys. Rev. Lett.* **70**, 3055 (1993).
- J. Feng, *Opt. Lett.* **18**, 1302 (1993).
- J. W. Fleischer, M. Segev, N. K. Efremidis, and D. N. Christodoulides, *Nature* **422**, 147 (2003).
- O. Cohen, T. Schwartz, J. W. Fleischer, M. Segev, and D. N. Christodoulides, *Phys. Rev. Lett.* **91**, 113901 (2003).
- J. Meier, J. Hudock, D. Christodoulides, G. Stegeman, Y. Silberberg, R. Morandotti, and J. Aitchison, *Phys. Rev. Lett.* **91**, 143907 (2003).
- Z. Chen, A. Bezryadina, I. Makasyuk, and J. Yang, *Opt. Lett.* **29**, 1656 (2004).
- X. Fan, G. P. Wang, J. C. W. Lee, and C. Chan, *Phys. Rev. Lett.* **97**, 073901 (2006).
- Y. Liu, G. Bartal, D. A. Genov, and X. Zhang, *Phys. Rev. Lett.* **99**, 153901 (2007).
- A. Marini, A. V. Gorbach, and D. V. Skryabin, *Opt. Lett.* **35**, 3532 (2010).
- F. Ye, D. Mihalache, B. Hu, and N. C. Panoiu, *Phys. Rev. Lett.* **104**, 106802 (2010).
- Y. Kou, F. Ye, and X. Chen, *Phys. Rev. A* **84**, 033855 (2011).
- C. Huang, X. Shi, F. Ye, Y. V. Kartashov, X. Chen, and L. Torner, *Opt. Lett.* **38**, 2846 (2013).
- Y. Kou, F. Ye, and X. Chen, *Opt. Lett.* **38**, 1271 (2013).
- Y. Xue, F. Ye, D. Mihalache, N. C. Panoiu, and X. Chen, *Laser Photonics Rev.* **8**, L52 (2014).
- C. Huang, F. Ye, Z. Sun, and X. Chen, *Opt. Express* **22**, 30108 (2014).
- S. Longhi and K. Staliunas, *Opt. Commun.* **281**, 4343 (2008).
- S. Longhi, *Opt. Lett.* **35**, 235 (2010).
- F. Dreisow, A. Szameit, M. Heinrich, T. Pertsch, S. Nolte, A. Tünnermann, and S. Longhi, *Phys. Rev. Lett.* **102**, 076802 (2009).
- A. A. Sukhorukov and Y. Kivshar, *Opt. Lett.* **27**, 2112 (2002).
- A. A. Sukhorukov and Y. S. Kivshar, *Phys. Rev. Lett.* **91**, 113902 (2003).
- A. A. Sukhorukov and Y. Kivshar, *Opt. Lett.* **28**, 2345 (2003).
- M. I. Molina, I. L. Garanovich, A. A. Sukhorukov, and Y. S. Kivshar, *Opt. Lett.* **31**, 2332 (2006).
- R. Morandotti, D. Mandelik, Y. Silberberg, J. S. Aitchison, M. Sorel, D. N. Christodoulides, A. A. Sukhorukov, and Y. S. Kivshar, *Opt. Lett.* **29**, 2890 (2004).
- D. Mihalache, D. Mazilu, Y. Kivshar, and F. Lederer, *Opt. Express* **15**, 10718 (2007).
- P. B. Johnson and R. W. Christy, *Phys. Rev. B* **6**, 4370 (1972).
- S. Hyun Nam, E. Ulin-Avila, G. Bartal, and X. Zhang, *Opt. Lett.* **35**, 1847 (2010).
- A. Zoubir, M. Richardson, C. Rivero, A. Schulte, C. Lopez, K. Richardson, N. Hô, and R. Vallée, *Opt. Lett.* **29**, 748 (2004).